Available online at www.sciencedirect.com
SCIENCE DIRECT
International Journal of Mass Spectrometry 249–250 (2006) 162–170
International Journal of Mass Spectrometry
www.elsevier.com/locate/ijms

Surface-induced dissociation and reactions of dications and cations: Collisions of dications $C_7H_8^{2+}$, $C_7H_7^{2+}$, and $C_7H_6^{2+}$ and a comparison with the respective cations $C_7D_8^{\bullet+}$ and $C_7H_7^{+}$

J. Jašík [a,1], J. Roithová [a], J. Žabka [a], A. Pysanenko [a], L. Feketeová [b,2], I. Ipolyi [a,1], T.D. Märk [b], Z. Herman [a,b,*]

[a] *V. Čermák Laboratory, J. Heyrovský Institute of Physical Chemistry, Academy of Sciences, Dolejškova 3, 18223 Prague 8, Czech Republic*
[b] *Institut für Ionenphysik, Leopold-Franzens Universität, Techniker Str. 25, A-6020 Innsbruck, Austria*

Received 30 September 2005; received in revised form 21 December 2005; accepted 27 December 2005
Available online 7 February 2006

Abstract

Collisions of cations and dications $C_7H_8^{+/2+}$, $C_7H_7^{+/2+}$, and $C_7H_6^{2+}$ generated by electron ionization of toluene with a highly oriented pyrolytic graphite surface were investigated in scattering experiments at the incident energy of 25.3 eV, incident angle of 60° (with respect to the surface normal) and at surface temperatures of 300 and 900 K. The survival probability of ions was rather large, about 10% for the cations and about twice as large for the dications. Only singly-charged ions were observed in the mass spectra of product ions for both singly- and doubly-charged incident ions. In agreement with earlier conclusion of Cooks et al., the primary process in surface collisions of the dications is a single-charge exchange between the approaching dication and the surface at larger distances; hence, the mass spectrum of product ions in fact results from surface interactions of internally excited monocations. This scenario is also supported by measured translational energy distributions and angular distributions of the major product ions which are very similar for both dication- and cation-collisions. Two mechanisms of formation for the fragment ions observed are suggested: either via unimolecular decomposition of the inelastically scattered projectile ion or via decay of the protonated projectile formed by endoergic hydrogen transfer from the surface hydrocarbons to the projectile ion. The translational energy distributions of ions originating from dissociation of the surface-excited projectile ions peak at higher energies than those of the ions resulting from decomposition of surface-protonated precursor ions.

Keywords: Dications; Toluene; Scattering experiments; Surface-induced dissociation; Surface reactions

1. Introduction

Studies on interactions between hyperthermal ions and surfaces have developed recently from a purely fundamental physics area of research to a branch of science of interest to both physicists and chemists. Considerable effort has been devoted over the last two decades to investigations of selected physical and chemical processes stimulated by impact of ions with energy of 5–100 eV on surfaces [1–5]. These studies find many applications in science and technology ranging from surface diagnostics and surface modification to characterization of projectile ions. In particular, surface-induced dissociation (SID) of ions has been successfully used as one of the methods for characterizing structural properties of polyatomic organic or bioorganic ion projectiles [3,4]. For these studies, the ion survival probability in ion-surface collisions plays an important role.

In this communication we report on a comparison of ion-surface interactions of polyatomic cations with their respective dications. The ions $C_7H_8^{+/2+}$, $C_7H_7^{+/2+}$, and $C_7H_6^{2+}$ are used as projectiles, because (i) they are generated in sufficient amounts by electron ionization (EI) of toluene [6] and (ii) mass-selection of the dications (*m*/*z* 46, 45.5, and 45) is not disturbed by isobaric impurities of other singly-charged ions generated from

* Corresponding author. Tel.: +420 2 66 053 514; fax: +420 2 86 582 307.
E-mail address: zdenek.herman@jh-inst.cas.cz (Z. Herman).
[1] Pre-Doctoral Stipendist under the auspices of the EU Network MCI (Generation, Stability and Reaction Dynamics of Multiply-Charged Ions), 2002–2003. Present address: Department of Experimental Physics, Comenius University, Bratislava, Slovak Republic.
[2] Visitor to the J. Heyrovsky Institute under the cooperation programme Association EURATOM-IPP.CR and Association EURATOM-OAW.

1387-3806/$ – see front matter © 2006 Elsevier B.V. All rights reserved.
doi:10.1016/j.ijms.2005.12.043

toluene. The effects of charge of the projectile ions on the ion survival probability and the surface-induced dissociations are investigated in a series of scattering experiments, in which mass spectra, angular and translational energy distributions of product ions resulting from surface collisions of both singly- and doubly-charged ions have been measured. Mass spectra of product ions from interaction of the above mentioned doubly- and singly-charged ions with a metal surface were studied earlier at the incident energy of 44 eV by Cooks and co-workers [7]. Only singly-charged ions were observed as products of surface collisions of the dications and it was concluded that charge transfer and dissociative charge transfer were the dominant processes. Similarities of the mass spectra of the corresponding dication- and cation-projectiles were interpreted as an indication that the reaction sequence at the surface was charge transfer followed by dissociation.

2. Experimental

The beam scattering apparatus EVA II, modified for ion-beam surface scattering studies [5,8–13], was used in the present experiments. Briefly, projectile cations and dications were formed by electron ionization (120 eV) of toluene. The ions were then extracted, accelerated to about 140–300 eV, mass-selected by a 90° permanent magnet, and decelerated to the required energy in a multi-element deceleration lens. The resulting projectile-ion beam had an energy spread of 0.2 eV, full-width-at-half-maximum (FWHM), an angular spread of 1°, FWHM, and geometrical dimensions of 0.4 mm × 1.0 mm. The ion beam was directed towards the target surface under a pre-adjusted incident angle Φ_N. Ions scattered from the surface passed through a detection slit (0.5 mm × 1 mm), located 25 mm from the target, into a stopping-potential energy analyzer. In the next step, the ions were accelerated by a potential of 1000 V, mass-analyzed in a magnetic sector, and detected with a Galileo channel multiplier. The exit slit of the projectile beam, the target, and the detection slit were kept at the same potential during the experiments and this equipotential region was shielded by μ-metal sheets. The projectile beam–target section could be rotated about the scattering center with respect to the detection slit to obtain angular distributions. In the experiments described here the impact angle of the projectile ions was set at $\Phi_N = 60°$ with respect to the surface normal (30° with respect to the surface.) The surface used in this study was a highly oriented pyrolytic graphite (HOPG) sample. The surface at room temperature was covered by a layer of hydrocarbons, as shown earlier [9,11–13]. For comparison, collisions with a heated surface were studied, too. In these experiments, the target was heated to about 600 °C [9]; the heating led to a depletion of the hydrocarbon layer by more than 100 times [9].

3. Results and discussion

3.1. Ion survival probability

The absolute ion survival probability S_a (percentage of all ions surviving the surface collision as product ions) was determined similarly as in our previous studies [9,13]. It is defined as the ratio of the sums of intensities of all product ions scattered from the surface, $\sum I_{PT}$, divided by the intensity of the projectile-ion beam incident on the surface, I_{RT}, $S_a = 100 \sum I_{PT}/I_{RT}$. The values that can be directly measured are I_{RT}, the intensity of the projectile ion beam incident on the target, and $\sum I_{PD}$, sum of the intensities of product ions reaching the detector (from mass spectra of product ions). Their ratio defines the experimentally accessible effective survival probability $S_{eff} = \sum I_{PD}/I_{RT}$. The value of $\sum I_{PT}$ cannot be directly measured and must be estimated from $\sum I_{PD}$, by taking into account the apparatus discrimination and the angular discrimination of the experiment. Details of the procedure of obtaining both angular and apparatus discrimination factors and approximations involved in it were described earlier [9,13]. The final expression is $S_a = FS_{eff} = F\sum I_{PD}/I_{RT}$, where both $\sum I_{PD}$ and I_{RT} are measurable quantities and all discriminating factors are contained in F ($\sum I_{PD}$ is in counts per seconds (cps) recalculated to the ion current, I_{RT} takes into account the double-charge of the projectile ions). In the present experiments, the factor F was determined from the available data as $F = 1.8 \times 10^4$. (Note that in our earlier studies [9,13] product ion currents were measured on the output of the multiplier rather than counted; the factor F included multiplication of the multiplier and therefore its value was by about 5 orders of magnitude smaller than here.)

The presently obtained survival probabilities for the dications projectiles at the incident energy of 25.3 eV are $S_a(C_7H_8^{2+}) = 20 \pm 7\%$, $S_a(C_7H_7^{2+}) = 23 \pm 4\%$, $S_a(C_7H_6^{2+}) = 32 \pm 7\%$; for the cation projectiles $S_a(C_7H_8^{+}) = 11 \pm 2\%$, and $S_a(C_7H_7^{+}) = 14 \pm 4\%$. The relative error shown here was estimated as the standard deviation of a series of usually five measurements of I_{RT} on the target and I_{PD} in the corresponding mass spectra. As stated earlier [9,13], due to approximations in estimating F, the values of S_a are presumably close to the upper limit of the ion survival probability.

The survival probabilities of the dications are about twice as large as those of the respective cations. The survival probabilities of the cations $C_7D_8^{\bullet+}$ and $C_7H_7^{+}$ are comparable to those obtained for closed-shell small hydrocarbon ions, though $C_7D_8^{\bullet+}$ is a radical cation. For the previously studied closed-shell cations (CH_5^{+} [9] or $C_2H_3^{+}$ [13]) the survival probabilities of about 3–15% were reported, while for many open-shell radical cations (e.g., $CH_4^{\bullet+}$ [9] or $C_2H_2^{\bullet+}$ [13]) S_a was found to be less than 1%. The large survival probabilities of $C_7D_8^{\bullet+}$ and $C_7H_7^{+}$ may be due to their rather low recombination energies (usually similar to the ionization energies, IE); e.g., IE of toluene is 8.83 eV [14] and IE of tropylium radical $C_7H_7^{\bullet}$ is 6.28 eV [15]. Hence, these values are lower than the effective ionization energies of hydrocarbons on the surface (estimated to be about 10–11 eV).

3.2. Mass spectra and velocity distributions of product ions

3.2.1. $C_7H_8^{\bullet+}$ and $C_7H_8^{2+}$

The SID mass spectra of the dications $C_7H_8^{2+}$, $C_7H_7^{2+}$, and $C_7H_6^{2+}$ and of the cations $C_7H_8^{\bullet+}$ and $C_7H_7^{+}$ are shown at Fig. 1. The mass resolution of the spectra was fairly low

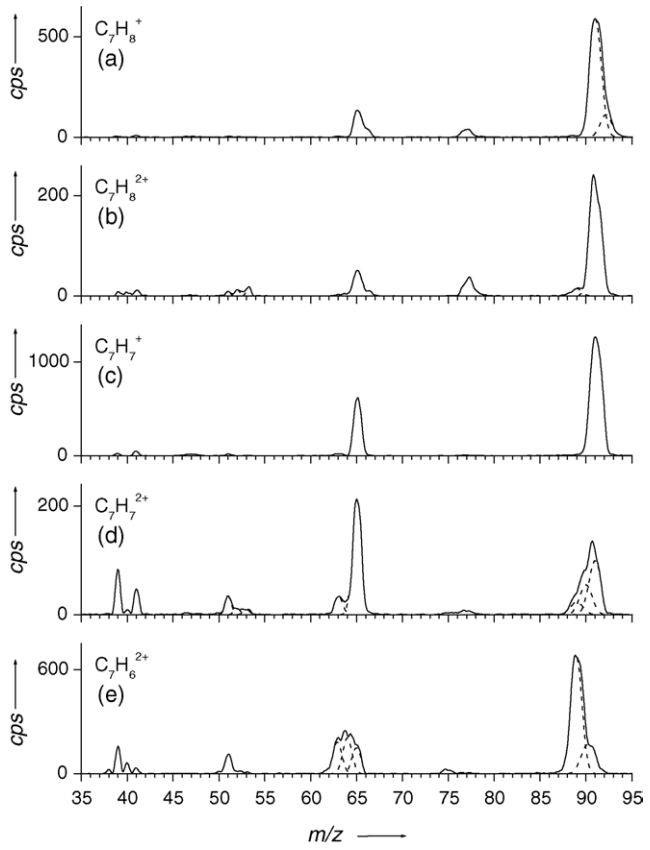

Fig. 1. Mass spectra of product ions from surface interaction of $C_7H_8^{\bullet+}$ (a), $C_7H_8^{2+}$ (b), $C_7H_7^{+}$ (c), $C_7H_7^{2+}$ (d), $C_7H_6^{2+}$ (e). Ions generated by EI of toluene, HOPG surface with a hydrocarbon layer, incident energy 25.3 eV, incident angle with respect to the surface normal $\Phi_N = 60^\circ$.

due to a large energy spread of the product ions (see later on). Some of the product ion signals had to be deconvoluted. This was done by a careful simulation of repeated recordings of the respective portions of the mass spectra (only the final result is shown in Fig. 1). The reliability of the deconvoluted peak heights was sufficient for the present discussion of the results.

The spectra of doubly-charged precursor ions consist of only singly-charged product ions. This finding is in agreement with the previously published conclusion that electron transfer precedes interaction of the dications with the surface [7]. Thus, the SID spectrum of a dication should closely resemble the spectrum of a corresponding singly-charged ion. Possible differences then follow from different structures of the precursor ions, monocations and dications, respectively, or different internal energies. The mass spectra in Fig. 1 are indeed quite similar for both monocations and dications. Nevertheless, it can be seen that the extent of fragmentation is more pronounced for the cations formed from doubly-charged precursor ions.

As repeatedly reported [8], the scattering of radical cations at surfaces covered with hydrocarbons is partly associated with abstraction of a hydrogen atom from the surface and formation of a protonated projectile ion. Thus, one has to take into account that the SID spectrum of the toluene cation (Fig. 1(a)) may involve fragmentation of both $C_7H_8^{\bullet+}$ and $C_7H_9^{+}$ ions.

First, the fragmentation of $C_7H_8^{\bullet+}$ will be addressed. The majority of mass-selected projectile-ions $C_7H_8^{\bullet+}$ formed by electron ionization of toluene can be assumed to retain the connectivity of toluene ($TOL^{\bullet+}$), because the ions with sufficiently high internal energy to undergo skeletal rearrangements decompose and form either the benzyl cation (Bz^+) or the tropylium ion (Tr^+) prior to the surface collision [16]. In agreement with this finding, the mass spectrum of product ions from surface interaction of $C_7H_8^{\bullet+}$ (Fig. 1(a)) is dominated by a loss of a hydrogen atom that leads to Bz^+ or Tr^+. The next abundant fragmentations in electron mass spectra of toluene yield the group of $C_5H_x^+$ fragment ions ($x = 1$–6) [17], typically dominated by $C_5H_5^+$ (m/z 65) followed by $C_5H_3^+$ (m/z 63). Accordingly, a fragmentation channel leading to $C_5H_5^+$ was detected in the SID of $C_7H_8^{\bullet+}$. Other less abundant channels lead to C_3-, C_4-, and C_6-fragments.

The structure of the ion $C_7H_9^+$ formed from toluene was studied experimentally [17]. It was concluded that the major fraction of $C_7H_9^+$ ions retain the connectivity of the σ-complex [18] of the protonated toluene molecule, whereas a minor fraction of ions undergoes a reversible expansion of the ring to protonated 1,3,5-cycloheptatriene. The dominant fragmentation channel of protonated toluene leads to a loss of the hydrogen molecule concomitant with the formation of $C_7H_7^+$ (m/z 91). Hence, the dominant fragmentation channel of both $C_7H_8^{\bullet+}$ and $C_7H_9^+$ leads to the same fragment ion. The second most abundant process in the fragmentation of $C_7H_9^+$ is elimination of methane coinciding with a loss of a methyl radical from $C_7H_8^{\bullet+}$, both leading to fragment ion $C_6H_5^+$ (m/z 77). Nevertheless, in the SID spectra of $C_7H_8^{\bullet+}$ the intensity of the ion of m/z 77 is unusually large (Fig. 1) with respect to the negligible abundance of C_3- and C_4-fragments, if only fragmentation of $C_7H_8^{\bullet+}$ is considered. Therefore, it can be expected that a significant part of the $C_6H_5^+$ ions arises from the fragmentation of protonated toluene. The presence of protonated toluene can be also responsible for a rather large abundance of $C_5H_6^+$ (m/z 66).

Further evidence for involvement of protonated toluene in the SID spectra of the toluene molecular ion can be obtained from experiments with perdeuterated toluene. The reaction of the incident $C_7D_8^{\bullet+}$ ion at the surface yields the $C_7D_8H^+$ ion. In its fragmentation, either a perdeuterated fragment or a fragment containing the hydrogen atom coming from the surface can be lost. Fig. 2(a) shows the SID spectrum of $C_7D_8^{\bullet+}$. The mass region corresponding to the loss of a methyl radical from $C_7D_8^{\bullet+}$ or methane from $C_7D_8H^+$ shows a rather convincing result: there is a peak at the odd mass m/z 81 ($C_6D_4H^+$) which can come only from fragmentation of $C_7D_8H^+$. The $C_6D_4H^+$ fragment is more abundant than $C_6D_5^+$ (m/z 82), in agreement with the statistical priority of the CD_4 loss as compared to the CD_3H loss from $C_7D_8H^+$. However, the fragment $C_6D_5^+$ can be also formed by a loss of a methyl radical from $C_7D_8^{\bullet+}$. The relatively small abundance of $C_6D_5^+$ in the SID spectra suggests that this process is not important and therefore the C_6-fragments originate prevailingly from the fragmentation of the protonated projectiles.

As to the formation of $C_7H_9^+$ itself, two possible scenarios can be put forward: (i) either the singly-charged projectile

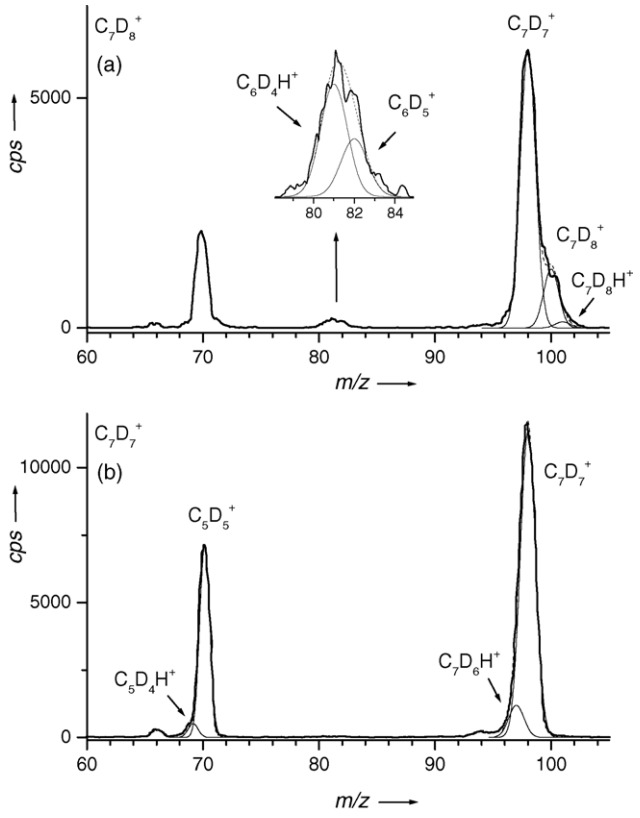

Fig. 2. Mass spectra of product ions from interaction of $C_7D_8^{\bullet+}$ (a) and $C_7D_7^+$ (b) projectile ions generated by EI of D_8-toluene (HOPG surface with a hydrocarbon layer, incident energy 25.3 eV, and incident angle $\Phi_N = 60^\circ$).

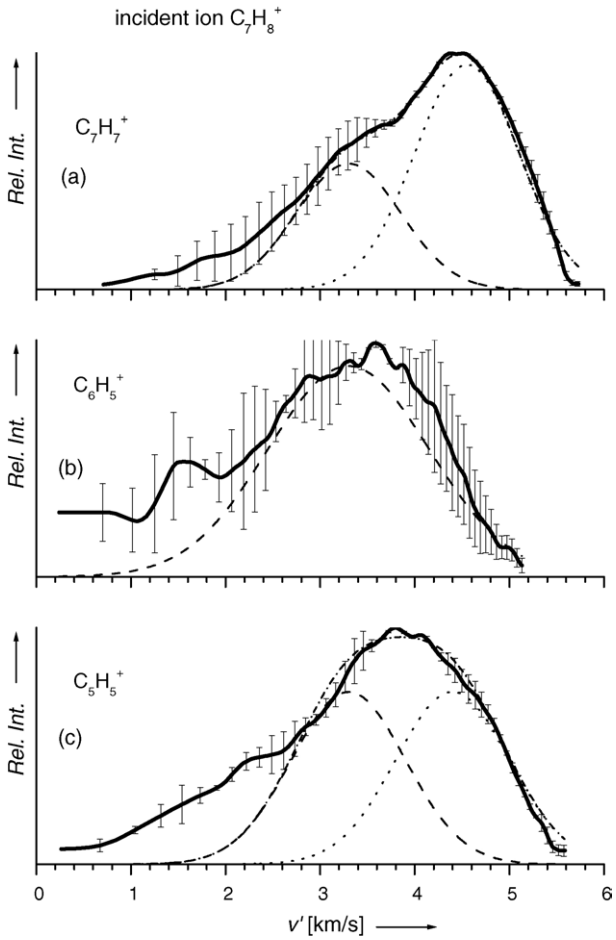

Fig. 3. Velocity distributions of the product ions $C_7H_7^+$ (a), $C_6H_5^+$ (b), and $C_5H_5^+$ (c) from collisions of $C_7H_8^{\bullet+}$ with hydrocarbon-covered HOPG surface at room temperature (incident energy 25.3 eV, incident angle $\Phi_N = 60^\circ$). The velocity distributions were simulated by Gaussian peaks as discussed in the text.

abstracts a hydrogen atom from surface hydrocarbons (reaction (1)) or (ii) the projectile undergoes neutralization on the surface and in the second step it is reionized by the proton transfer from the ionized surface hydrocarbons (reaction sequence (2)).

$$C_7H_8^{\bullet+} + \text{H-CH}_2\text{-S} \rightarrow C_7H_9^+ + {}^\bullet\text{CH}_2\text{-S} \quad (1)$$

$$C_7H_8^{\bullet+} + \text{H-CH}_2\text{-S} \rightarrow C_7H_8 + {}^{\bullet+}\text{CH}_3\text{-S} \rightarrow C_7H_9^+ + {}^\bullet\text{CH}_2\text{-S} \quad (2)$$

From the point of view of energetics, both scenarios are equivalent. In the following we will calculate the energy balance for the mechanism represented by reaction (1). As mentioned above, the connectivity of the $C_7H_8^{\bullet+}$ ion corresponds to that of toluene. The overall $\Delta_r H$ can be estimated considering the two partial reaction Eqs. (3) and (4):

$$C_7H_8^{\bullet+} + H^\bullet \rightarrow C_7H_9^+ \quad (3)$$

$$\text{H-CH}_2\text{-S} \rightarrow H^\bullet + {}^\bullet\text{CH}_2\text{-S} \quad (4)$$

Thus, $\Delta_r H(3) = \Delta_f H(C_7H_9^+) - \Delta_f H(C_7H_8^{\bullet+}) - \Delta_f H(H^\bullet) = -3.34$ eV, where $\Delta_f H(C_7H_9^+) = \Delta_f H(\text{TOL}) + \Delta_f H(H^+) - \text{PA(TOL)} = 0.52\text{ eV} + 15.86\text{ eV} - 8.12\text{ eV} = 8.26\text{ eV}$ ([19–21], respectively), $\Delta_f H(H^\bullet) = 2.25$ eV [20], and $\Delta_f H(C_7H_8^{\bullet+}) = \Delta_f H(\text{TOL}) + \text{IE(TOL)} = 0.52\text{ eV} + 8.83\text{ eV} = 9.35\text{ eV}$. $\Delta_r H(4)$ can be estimated as an average bond-energy of the C–H bond in surface hydrocarbons, reported to be 413 kJ/mol (4.3 eV) [22]. Hence, the overall energy balance corresponds to an endoergicity of about 1 eV.

The energy defect can be covered from either internal or translational energy of the projectile ion. Therefore, it may be assumed that the translational energy of the ions that underwent reaction (1) should be smaller than of those that were "only" scattered.

Distributions of translational energy of the major scattered product ions transformed to the corresponding velocities of the ions are shown in Fig. 3. The distributions of ion velocities can be directly compared, because the daughter ions formed by unimolecular fragmentation from the parent ions should have similar velocity distributions, as shown earlier for surface-induced dissociation of a variety of polyatomic ions [2,5,8–12]. (On the other hand, the translational energy distributions are influenced by the masses of the corresponding ions). The velocity distributions in Fig. 3 are broad and exhibit a structure. Under the assumption that the fragment ions $C_7H_7^+$ originate from both $C_7H_8^{\bullet+}$ and $C_7H_9^+$, the corresponding velocity distribution (Fig. 3(a)) can be simulated by two Gaussian peaks with maxima at 3.30 (dashed line) and 4.55 km/s (dotted line). As discussed

above, the abstraction of a hydrogen atom from the surface is an endothermic reaction, therefore it is expected that the $C_7H_9^+$ ions or their fragments should have a lower translational energy than those originating from the scattered $C_7H_8^{\bullet+}$ ions. Thus, the peak at 4.55 km/s (Fig. 3(a)) may be assigned to the $C_7H_7^+$ ions formed by the dissociation of scattered $C_7H_8^{\bullet+}$, while the peak at 3.30 km/s may correspond to the loss of H_2 from $C_7H_9^+$. This reasoning is strongly supported by the velocity distribution of the $C_6H_5^+$ fragment ion (Fig. 3(b)), which is mostly represented by a peak at 3.30 km/s: as suggested by the labeling experiment, the $C_6H_5^+$ ion is mostly formed by a loss of methane molecule from protonated toluene $C_7H_9^+$. The velocity distribution of $C_5H_5^+$ (Fig. 3(c)) shows that this ion originates from both precursors. The low energy tails of the velocity distributions in all three cases may reflect the fragmentation of precursors in excited states, as the lower translational energy corresponds to a larger internal energy excitation, although other mechanisms, like a reaction at the surface, cannot be excluded, too. The velocity peak at 4.55 km/s corresponds to the translational energy of the surface-excited precursor ion $C_7H_8^{\bullet+}$ of 9.87 eV, and the velocity peak at 3.30 km/s corresponds to the translational energy of the precursor ion $C_7H_9^+$ of 5.25 eV. Thus, there is a difference in the translational energies of about 4.6 eV between the two precursor ions. An analogous behavior was observed earlier in our studies of surface-induced dissociation and reactions of the benzene cation $C_6H_6^+$ [10]. There the double-peaking of the energy and velocity distributions of the product ions was assigned, without further analysis of the energetics, to direct fragmentation of the projectile ions and to fragmentation of the surface-protonated projectiles formed in an endoergic reaction, respectively.

Interesting conclusions come from a comparison of results for singly- and doubly-charged projectile ions. It was suggested earlier that doubly-charged ions undergo charge transfer upon a collision with the surface [7]. Thus, the SID mass spectra of both $C_7H_8^{\bullet+}$ and $C_7H_8^{2+}$ reflect fragmentation of $C_7H_8^{\bullet+}$. However, whereas the structure of the $C_7H_8^{\bullet+}$ projectile corresponds almost exclusively to that of the toluene cation ($TOL^{\bullet+}$), various isomers may be present in the $C_7H_8^{2+}$ dication beam. The most stable isomer corresponds to the *meta*-protonated benzyl cation, followed by the *ortho*-protonated benzyl cation, and the protonated tropylium ion, respectively [23]. The fragmentation of these structures is not sufficiently specific. We can only state that the precursor ions formed after charge exchange in the surface interaction of the incident $C_7H_8^{2+}$ dications have larger internal energies, as evidenced by a larger abundance of the lower mass C_3- and C_4-fragment ions than in the spectra of the $C_7H_8^{\bullet+}$ projectile (Fig. 1(b)). The mass spectrum of the products of the $C_7H_8^{2+}$ dication collisions with the surface suggests again formation of $C_7H_9^+$ (as implied by high abundance of $C_6H_5^+$ and $C_5H_6^{\bullet+}$ product ions).

Velocity distributions of fragment ions formed upon surface collisions of the projectile ion $C_7H_8^{2+}$ are shown in Fig. 4. The main feature of the distribution of the product $C_7H_7^+$ (Fig. 4(a)) may be simulated by an overlap of two Gaussian peaks with maxima at 4.65 (dotted line) and 3.90 km/s (dashed line). Due to a structural diversity and higher internal energies of the precursor

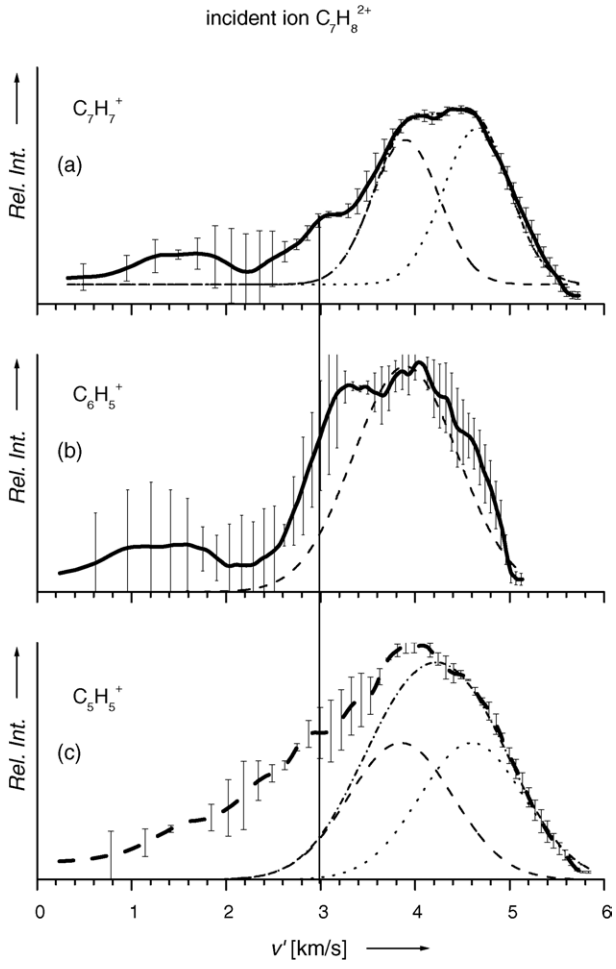

Fig. 4. Velocity distributions of the product ions $C_7H_7^+$ (a), $C_6H_5^+$ (b), and $C_5H_5^+$ (c) from the collisions of $C_7H_8^{2+}$ with hydrocarbon-covered HOPG surface at room-temperature (incident energy 25.3 eV, incident angle $\Phi_N = 60^\circ$). The velocity distributions were simulated by Gaussian peaks as discussed in the text.

ions, more pathways leading to the product ions are evidently possible. One of them can be discerned at the velocity of about 3.00 km/s, others at even lower velocities between about 1 and 2 km/s. Similarly as above, the high velocity peak at 4.65 km/s can be ascribed to the direct fragmentation of the surface-excited projectile ion, i.e., to the hydrogen loss from $C_7H_8^{\bullet+}$. The peak with a maximum at the velocity of 3.9 km/s can be ascribed to the hydrogen abstraction from the surface, namely to the fragmentation pathway $C_7H_8^{2+} \rightarrow C_7H_8^{\bullet+} \rightarrow C_7H_9^+ \rightarrow C_7H_7^+$. As there are essentially two isomers of $C_7H_8^{2+}$, the ring-protonated benzyl cation and the ring-protonated tropylium ion [23], two corresponding isomers of $C_7H_8^{\bullet+}$ are presumably formed by electron transfer at the surface. As a result, two isomers are likely to originate from the hydrogen abstraction from the surface, namely protonated toluene and protonated cycloheptatriene, respectively. Different pathways connected with the formation of these two isomers might be responsible for yet another translational energy loss indicated in the velocity distributions at 3.0 km/s. The velocity distributions of $C_6H_5^+$ and $C_5H_5^+$ in Fig. 4 may be interpreted in a similar way as those in Fig. 3.

3.2.2. $C_7H_7^+$, $C_7H_7^{2+}$, and $C_7H_6^{2+}$

It can be expected that the interaction of $C_7H_7^+$, $C_7H_7^{2+}$, and $C_7H_6^{2+}$ ions with the surface will be by and large analogous to that of $C_7H_8^{\bullet+}$ and $C_7H_8^{2+}$. The mass spectra of the $C_7H_7^+$ and $C_7H_7^{2+}$ projectile ions (Fig. 1(c and d), respectively) are dominated by the formation of the stable ion $C_5H_5^+$. Due to a higher internal energy of the scattered precursor ions formed from doubly-charged projectiles, the SID spectrum of $C_7H_7^{2+}$ shows more pronounced fragmentation. A similar fragmentation pattern can be observed for $C_7H_6^{2+}$ (Fig. 1(e)), too, except that the C_5-fragments ions are present as $C_5H_3^+$, $C_5H_4^{\bullet+}$, and $C_5H_5^+$ of comparable intensities. Similarly as with $C_7H_8^{\bullet+}$, the mass spectra of the surface-scattered projectile ions $C_7H_7^+$ may represent an overlap of fragmentation of the surface-excited cations and of the ions formed by hydrogen abstraction from the surface (reaction (5)). To pursue this aspect in more detail, an experiment with the labeled incident ion $C_7D_7^+$ was carried out (Fig. 2(b)). As in the case of $C_7H_8^{\bullet+}$, the spectrum indicates formation of fragments containing a hydrogen atom from the surface ($C_7D_6H^+$ and $C_5D_4H^+$).

$$C_7H_7^+ + \text{H-CH}_2\text{-S} \rightarrow C_7H_8^{\bullet+} + {}^{\bullet}\text{CH}_2\text{-S} \quad (5)$$

$$C_7H_7^+ + H^{\bullet} \rightarrow C_7H_8^{\bullet+} \quad (6)$$

The energy balance of reaction (5) depends on the structure of the $C_7H_7^+$ ion. For the reaction of the benzylium ion with $H^{\bullet}$ to form the toluene cation, $\Delta_r H(5)$ can be estimated as the sum of $\Delta_r H(4) = 4.3$ eV (see above) and $\Delta_r H(6) = \Delta_f H(\text{TOL}^{\bullet+}) - \Delta_f H(H^{\bullet}) - \Delta_f H(\text{Bz}^{\bullet}) - \text{IE}(\text{Bz}^{\bullet}) = 9.35\,\text{eV} - 2.25\,\text{eV} - 2.15\,\text{eV}$ [24] $- 7.24\,\text{eV}$ [25] $= -2.24$ eV. The overall endoergicity is then equal to 2.1 eV. For the reaction of the tropylium ion with $H^{\bullet}$ leading to the cycloheptatriene cation, the energy balance of reaction (6) can be estimated as $\Delta_r H(6) = \Delta_f H(\text{CHT}^{\bullet+}) - \Delta_f H(H^{\bullet}) - \Delta_f H(\text{Tr}^+) = \Delta_f H(\text{CHT}^{\bullet+}) - \Delta_f H(H^{\bullet}) - (\Delta_f H(\text{CHT}^{\bullet+}) + \text{PA}(\text{Tr}^{\bullet}) - \Delta_f H(H^+) + \text{IE}(\text{Tr}^{\bullet})) = -\text{PA}(\text{Tr}^{\bullet}) + \text{IE}(H^{\bullet}) - \text{IE}(\text{Tr}^{\bullet}) = -8.62$ [21] $+ 13.60$ [26] $- 6.28$ [15] $= -1.30$ eV. This value in turn leads to the endoergicity of the H-atom transfer reaction (5) of 3.0 eV.

Fig. 5 shows velocity distributions of product ions from collisions of $C_7H_7^+$ (solid line) and $C_7H_7^{2+}$ (dashed line) with the surface. Similarly as with $C_7H_8^{\bullet+}/C_7H_8^{2+}$, the broad energy distribution can be explained by the involvement of at least two processes: a direct unimolecular fragmentation of the surface-excited projectile ion, and a hydrogen abstraction from the surface, formation of a protonated precursor ion, followed by its fragmentation. The two processes are indicated in the velocity spectra with the two vertical lines at 4.6 and 3.4 km/s, respectively. The velocity difference between these two values corresponds to a difference of 4.5 eV in translational energy. The positions of the two peaks in the velocity spectra and their mutual difference are similar as in the case of the $C_7H_8^{\bullet+}$ collisions. Note also that the maximum of the high-velocity peak, i.e., the peak corresponding to the direct fragmentation of the projectile ion, shifts to a lower value (~4.3 km/s) for the fragments $C_5H_5^+$ and $C_3H_3^+$, with respect to that of $C_7H_7^+$. This is consistent with the assumption that only the parent ions of higher internal energy content and thus of a lower translational

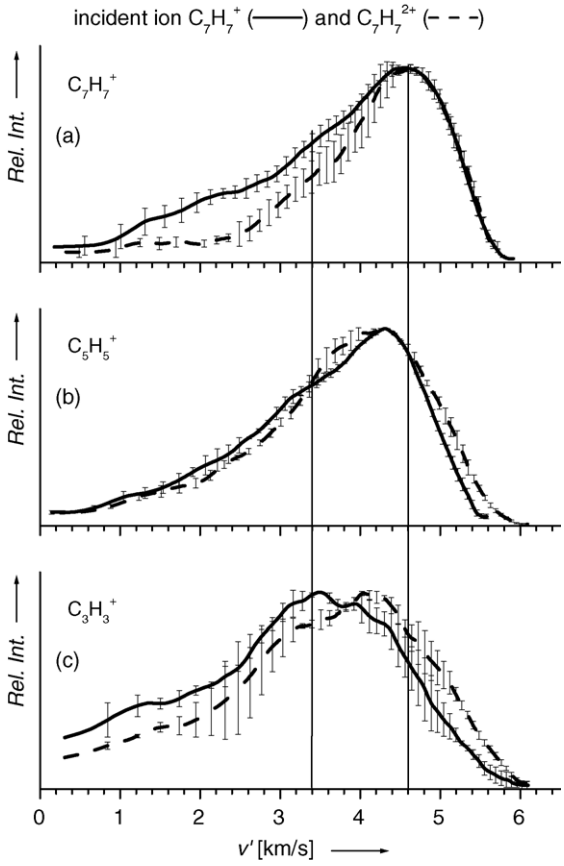

Fig. 5. Velocity distributions of the product ions $C_7H_7^+$ (a), $C_5H_5^+$ (b), and $C_3H_3^+$ (c) from the collisions of $C_7H_7^+$ (solid line) and $C_7H_7^{2+}$ (dashed line) with hydrocarbon-covered HOPG surface at room-temperature (incident energy 25.3 eV, incident angle $\Phi_N = 60°$). Vertical lines indicate two processes as discussed in the text.

energy undergo fragmentations. From the shape of the velocity distributions, it may be concluded that the direct fragmentation pathway of the surface-excited projectiles prevails over the surface protonation pathway. The major direct fragmentation process of the surface-excited $C_7H_7^+$ ion leads to $C_5H_5^+$. This fragment ion can also result from the surface reaction leading to $C_7H_8^{\bullet+}$ and its consecutive decomposition. The surface protonated projectile may also contribute to the abundance of $C_7H_7^+$ by a reverse loss of a hydrogen atom from $C_7H_8^{\bullet+}$ (intensity close to velocities at about 3–3.5 km/s). The fragment ion $C_3H_3^+$ can originate both from $C_7H_7^+$ and $C_7H_8^{\bullet+}$, with the $C_7H_8^+$ channel slightly prevailing. These findings are in agreement with the SID spectrum of the perdeuterated projectile $C_7D_7^+$ (Fig. 2(b)).

Due to sufficient intensities of product ions from surface interactions of $C_7H_7^+$, an experiment with the heated surface, i.e., with the hydrocarbon layer effectively removed, could be performed (the perdeuterated $C_7D_7^+$ projectile was used in this experiment). Fig. 6 shows a comparison of the translational energy distribution of the $C_7D_7^+$ product ions scattered from the surface at room temperature (a) and those scattered from the heated surface (b). Collisions with the heated, hydrocarbon-free carbon surfaces are known to be less inelastic than collisions

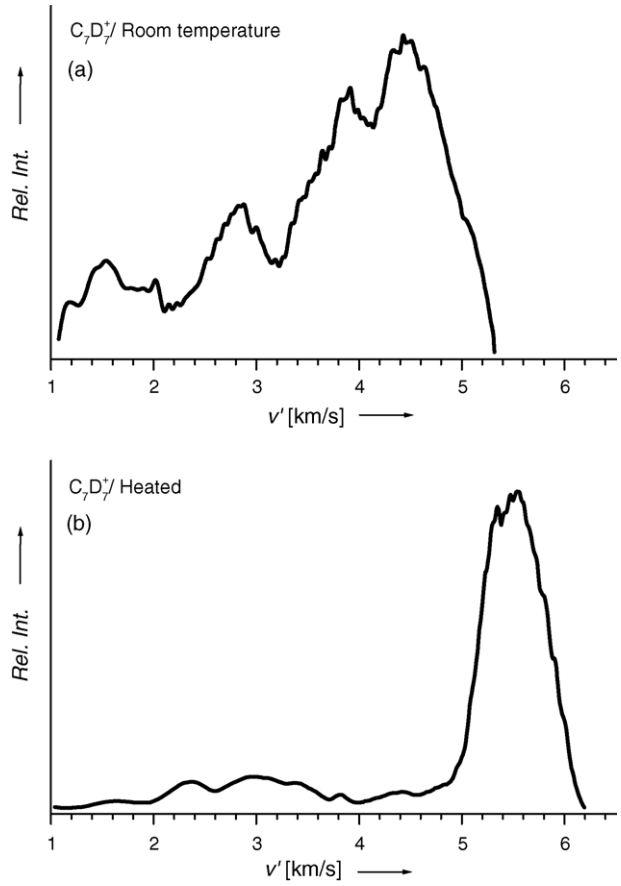

Fig. 6. Velocity distributions of the product ions $C_7D_7^+$ from collisions of $C_7D_7^+$ with the HOPG surface at room temperature (hydrocarbon-covered) (a) and heated to 600 °C (without the hydrocarbon layer) (b). Incident energy 25.3 eV, incident angle $\Phi_N = 60°$.

with surfaces covered at room temperature with hydrocarbons [9,13]. In agreement with this earlier finding, there is an evident change in the peak position corresponding to inelastically scattered undissociated $C_7D_7^+$ in the velocity distribution of the product ions: the peak shifts from 4.5 to 5.5 km/s (Fig. 6).

However, an important result comes from different widths of the velocity distributions. At room temperature, the components at lower velocities can be ascribed to the product ions resulting from surface reactions (see preceding Section 3). On the other hand, the distribution of velocities of product ions scattered from heated, i.e., practically hydrocarbon-free carbon surface, is narrow, devoid of any components at lower velocities. Thus, this result suggests that only direct inelastic scattering and dissociation of the projectile ion and no hydrogen-transfer reactions take place, as expected.

Finally, we note that the velocity distributions of the product ions formed from either singly- or doubly-charged precursor ions (both $C_7H_8^{+/2+}$ and $C_7H_7^{+/2+}$) are very similar. Our data provide no observable evidence for a possible surface-induced dissociation of the dications into a pair of two singly-charged ions. This process, often referred to as Coulomb explosion, is associated with a release of kinetic energy of several electronvolts, which should be seen in a broadening of the translational energy (velocity) distributions or angular distributions (Section 3.3) of the dications in comparison with the cations.

3.2.3. Translational energy loss of the protonation channel

The differences in the translational energy of the precursor ions resulting from inelastic scattering of the projectile ions and those resulting from hydrogen-transfer reaction at the surface are very similar. In the preceding paragraphs the value $\Delta E'_{tr} = 4.6$ eV was derived for $C_7H_8^{\bullet+}$, and $\Delta E'_{tr} = 4.5$ eV for $C_7H_7^+$. The inelastic scattering and direct fragmentation of the surface-excited projectile proceeds for both projectiles similarly as for other processes studied earlier with an overall inelasticity of 38% (in the other cases of polyatomic projectiles 30–38% [5,8–13]). However, the hydrogen-abstraction reactions have different endoergicities for the two projectiles (reactions (1) and (5)). The hydrogen abstraction by $C_7H_7^+$ is more endoergic (2–3 eV) than that by $C_7H_8^{\bullet+}$ (~1 eV). Assuming that the reaction endothermicity deficit is covered from the translational energy, this difference should be reflected in the velocity (translational energy) distributions. One may expect that the difference between the two peaks in the velocity distributions of products from the $C_7H_7^+$ projectile (Fig. 5) would be larger than that of products from the $C_7H_8^{\bullet+}$ projectile (Fig. 3). As the differences are almost the same, it appears that the loss of translational energy is not directly connected with the endoergicity of the hydrogen-transfer reaction, but rather that the barriers of the reactions or the properties of the surface may play a role. Hydrogen transfer from the surface hydrocarbons to the projectile is connected with a cleavage of a C–H bond, which requires energy of 4.3 eV [22] (see above). Thus the activation energy for the hydrogen-transfer reaction is close to the energy needed to break the C–H bond of surface hydrocarbons. It appears that the energy required to surmount the activation barrier is taken from the translational energy and therefore, a similar loss of translational energy is observed in the spectra of all projectiles and the process appears as projectile-independent.

Note, however, that the processes are complicated and the incident energy is distributed among internal and translational energy of products and the surface, therefore more factors may influence the final energy distributions.

3.3. Angular distributions of product ions

Finally, Fig. 7 summarizes the angular distributions of product ions from surface collisions of cations (solid line) and dications (dashed) $C_7H_8^{+/2+}$ and $C_7H_7^{+/2+}$. The product ions shown are the major dissociation products, the same as those for which the translational energy and velocity distributions are given in Figs. 3–5. Within the experimental error, the distributions are very similar for different fragment ions regardless of the charge of the incident ion. There is no indication of broadening of the distributions from collisions of the dication projectiles (possible effect of Coulomb repulsion in cation-pair formation). The distributions seem to peak universally at sub-specular angles, closer to the surface: for the incident angle of 60° the maximum of all product ion distributions is close to 74° and the width of

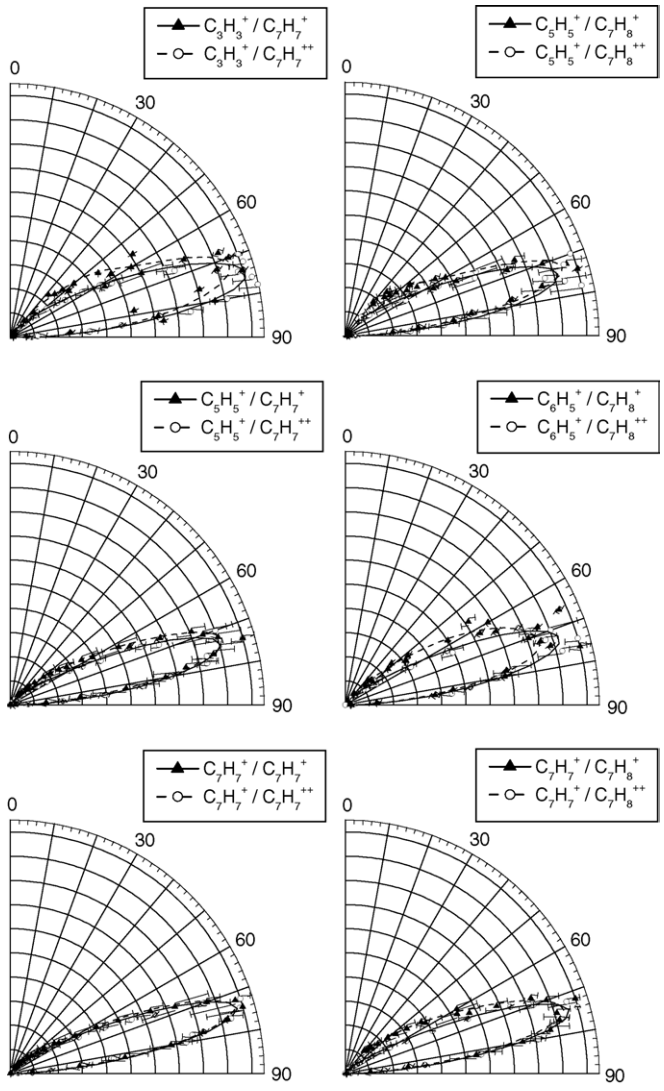

Fig. 7. Angular distributions of main product ions from collisions of $C_7H_7^+$ (solid lines) and $C_7H_7^{2+}$ (dashed lines) on the left, and from collisions of $C_7H_8^{\bullet+}$ (solid lines) and $C_7H_8^{2+}$ (dashed lines) on the right. Incident energy 25.3 eV, incident angle $\Phi_N = 60^\circ$.

the angular distributions is very similar for all measured product ions, 19–20°, full-width at half maximum.

4. Conclusions

1. Collisions of the cations and dications $C_7H_8^{+/2+}$, $C_7H_7^{+/2+}$, and $C_7H_6^{2+}$, formed by electron ionization of toluene, with highly oriented pyrolytic graphite surface, covered at room temperature with hydrocarbons, were investigated at the incident energy of projectile ions of 25.3 eV and incident angle of 60° with respect to the surface normal (30° with respect to the surface).
2. Mass spectra, translational energy distributions, and angular distributions of the product ions were measured. Only singly-charged product ions were observed at this incident energy. Translational energy distributions and angular distributions of the major product ions were very similar for both doubly- and singly-charged projectile ions. This suggests that the charge transfer between projectile-dications and the surface occurs at large distances and the collision events then reflect interactions of monocations with the surface. This conclusion is in agreement with the previous work of Cooks and co-workers [7].
3. Two possible fragmentation schemes were identified: fragmentations of the scattered cations M^+ corresponding to the projectile ions M^+/M^{2+} and fragmentations of ions $(M + H)^+$ coming from the reaction between the projectile ions and the surface hydrocarbons. This scenario was confirmed by isotope labeling experiments. The two mechanisms are reflected in translational energy distributions, where product ions resulting from endoergic hydrogen transfer reaction with surface hydrocarbons have smaller translational energies.
4. The survival probability, S_a, at this incident energy and incident angle was rather large, 11% and 14% for the cations $C_7H_8^+$ and $C_7H_7^+$, respectively, and 20–30% for the dications.

Acknowledgements

We dedicate this paper to the memory of Chava Lifshitz in deep respect to her personality and to her important contributions to the development of mass spectrometry. Partial support of this research by grants of the Grant Agency of the Academy of Sciences of the Czech Republic (Nos. 4040405 and KJB4040302), by the Research Center LC 510, by the Association EURATOM-IPP.CR in cooperation with Association EURATOM-ÖAW, and by EU Network MCI (Generation, Stability and Reaction Dynamics of Multiply-Charged Ions) is gratefully acknowledged.

References

[1] J.W. Rabalais (Ed.), Low Energy Ion-Surface Interactions, J. Wiley, New York, 1994.
[2] R.G. Cooks, T. Ast, M.D.A. Mabud, M. D. Int. J. Mass Spectrom. 100 (1990) 209.
[3] L. Hanley (Ed.), Polyatomic Ion-Surface Interactions, Int. J. Mass Spectrom. 174 (1994) 1.
[4] V. Grill, J. Shen, C. Evans, R.G. Cooks, Rev. Sci. Instrum. 72 (2001) 3149.
[5] Z. Herman, J. Am. Soc. Mass Spectrom. 14 (2003) 1360.
[6] B.P. Mathur, E.M. Burgess, D.E. Bostwick, T.F. Moran, Org. Mass Spectrom. 16 (1981) 92.
[7] M.D.A. Mabud, M.J. Dekrey, R.G. Cooks, T. Ast, Int. J. Mass Spectrom. 69 (1986) 277.
[8] J. Kubišta, Z. Dolejšek, Z. Herman, Eur. Mass Spectrom. 4 (1998) 311.
[9] J. Roithová, J. Žabka, Z. Dolejšek, Z. Herman, J. Phys. Chem. B 106 (2002) 8293.
[10] R. Wörgötter, J. Kubišta, J. Žabka, T.D. Märk, Z. Herman, Int. J. Mass Spectrom. Ion Process. 174 (1998) 53.
[11] J. Žabka, Z. Dolejšek, J. Roithová, V. Grill, T.D. Märk, Z. Herman, Int. J. Mass Spectrom. 213 (2002) 145.
[12] J. Žabka, Z. Dolejšek, Z. Herman, J. Phys. Chem. A 106 (2002) 10861.
[13] J. Jašík, J. Žabka, I. Ipolyi, L. Feketeová, T.D. Märk, Z. Herman, J. Phys. Chem. A 109 (2005) 10208.
[14] K.-T. Lu, G.C. Eiden, J.C. Weisshaar, J. Phys. Chem. 96 (1992) 9742.
[15] T. Koenig, J.C. Chang, J. Am. Chem. Soc. 100 (1978) 2240.
[16] C. Lifshitz, Acc. Chem. Res. 27 (1994) 138.

[17] R. Bombach, J. Dannacher, J.-P. Stadelmann, J. Am. Chem. Soc. 105 (1983) 4205.
[18] C.H. DePuy, R. Gareyev, S. Fornarini, Int. J. Mass Spectrom. Ion Process. 161 (1997) 41.
[19] H.Y. Afeefy, J.F. Liebman, S.E. Stein, in: P.J. Linstrom, W.G. Mallard (Eds.), NIST Chemistry WebBook, NIST Standard Reference Database Number 69, National Institute of Standards and Technology, Gaithersburg MD, June 2005, p. 20899 (http://webbook.nist.gov).
[20] M.W. Chase Jr., J. Phys. Chem. Ref. Data 9 (1998) 1.
[21] E.P. Hunter, S.G. Lias, J. Phys. Chem. Ref. Data 27 (1998) 413.
[22] M.W. Chase Jr., J. Phys. Chem. Ref. Data 9 (1998) 1.
[23] J. Roithová, D. Schröder, P. Gruene, T. Weiske, H. Schwarz, J. Phys. Chem. A, doi:10.1021/jp0545288, in press [Web Release date: 19-Nov-2005].
[24] W. Tsang, in: J.A. Martinho Simoes, A. Greenberg, J.F. Liebman (Eds.), Heats of Formation of Organic Free Radicals by Kinetic Methods in Energetics of Organic Free Radicals, Blackie Academic and Professional, London, 1996, p. 22.
[25] H.S. Im, E.R. Bernstein, J. Chem. Phys. 95 (1991) 6326.
[26] S.G. Lias, in: P.J. Linstrom, W.G. Mallard (Eds.), NIST Chemistry WebBook, NIST Standard Reference Database Number 69, National Institute of Standards and Technology, Gaithersburg MD, March 2003, p. 20899 (http://webbook.nist.gov).